A Satellite Freed of all but Gravitational Forces: "TRIAD I"

STAFF OF THE SPACE DEPARTMENT
The Johns Hopkins University Applied Physics Laboratory, Silver Spring, Md.
AND
STAFF OF THE GUIDANCE AND CONTROL LABORATORY
Stanford University, Stanford, Calif.

Under the sponsorship of the U.S. Navy, we have collaborated in the design of a "drag-free" satellite; a satellite in which surface forces (drag and radiation pressure) are cancelled by jets. The satellite was launched into a polar orbit on Sept. 2, 1972. The surface-force cancellation system performed faultlessly for more than a year. The satellite and its in-orbit performance are described.

I. Introduction and Summary

As part of an on-going effort to improve navigation by satellite, the U.S. Navy sponsored the experimental TRIAD satellite.

An important experiment aboard the satellite is a DISturbance (or surface force) COmpensation System (DISCOS). This system was first proposed about 10 years ago.[1] The basic idea is that a tiny satellite is completely enclosed in a cavity of a larger satellite. The inner satellite (or proof mass) is shielded from all external surface forces, drag and radiation pressure. As a part of the design it is necessary to:

1) eliminate all possible force interactions, including mass attraction, between the two bodies;

2) sense the relative displacement between the two; and

3) use this displacement signal to modify the motion of the (outer) satellite. As a result, the satellite is constrained to the orbit of the proof mass which is free of all external surface forces.

If the control system and design were perfect, then the equations of motion of the satellite would be identical with that of the proof mass

$$\ddot{\bar{r}} = -\bar{\nabla}U$$

where U is the gravitational potential.

In the design we sought to limit departures from this ideal to accelerations of 10^{-11} g. The largest error sources were 1) the mass-attraction asymmetries between the proof mass and the near-parts of the satellite; and 2) the electrical attraction between the proof mass and the capacitive position-sensing plates. The satellite design was also influenced by errors due to 3) magnetic gradient forces, 4) residual gas in the proof mass cavity, and 5) temperature gradients.

The satellite mass is 86.6 kg. It was launched in a "collapsed" configuration; roughly a cylinder 1.6 m high, 0.75-m-diam (see Fig. 1). In orbit, it expanded into three bodies (a "TRIAD"). The center body, containing the DISCOS unit, is separated from the two end bodies by 2.7 m booms (see Fig. 2). The top body contains the power supply while the lower unit contains transmitter, receiver, telemetry, and antenna. This configuration was chosen to minimize the fabrication problems associated with controlling the mass-attraction asymmetries on the proof mass; and to take advantage of the simplicity of gravity-gradient stabilization. A small spinning wheel was included to enforce a 3-axis stabilization relative to a locally-level system of coordinates.

The proof mass and cavity are shown schematically but to scale in Fig. 3. The proof mass, 22 mm in diameter, resides in a 40 mm cavity. The proof mass is a 70/30 gold-platinum alloy

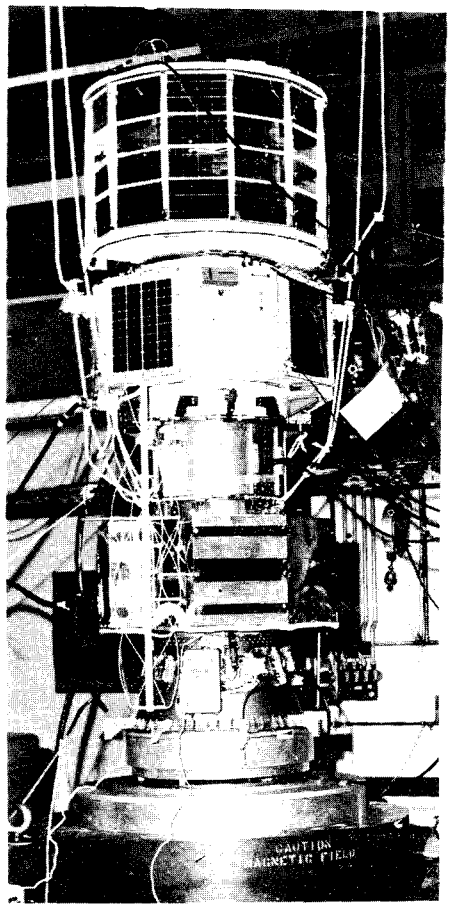

Fig. 1 TRIAD satellite in final stages of fabrication.

Presented as Paper 74-215 at the AIAA 12th Aerospace Sciences Meeting, Washington, D.C., January 30–February 1, 1974; submitted January 31, 1974; revision received May 20, 1974. This work was supported by the Department of the Navy under Navy Contract N00017-72-C-4401. The TRIAD satellite was designed and built in the Space Department of The Johns Hopkins University Applied Physics Laboratory. R. B. Kershner is the Department Head. J. Dassoulas is the Project Engineer. D. B. DeBra, Professor and Director of Guidance and Control Laboratory, Department of Aeronautics and Astronautics of Stanford University, was responsible for the design and fabrication of the DISCOS experiment.

Index categories: Earth Satellite Systems, Unmanned; Spacecraft Navigation, Guidance, and Flight-Path Control Systems.

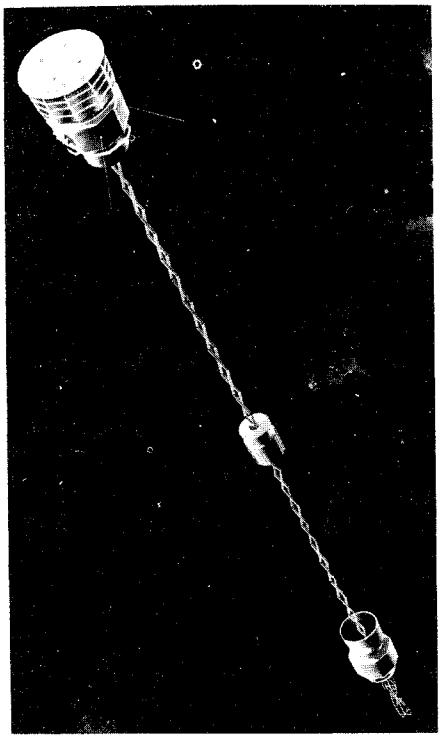

Fig. 2 TRIAD satellite in orbit (artist's rendition).

weighing 111 gm or 0.0013 of the satellite mass. This alloy was chosen for its high density and nearly zero magnetic susceptibility.

In orbit, the proof mass freely "floats" in the cavity; its position (relative to the cavity) is sensed by a set of 3 capacitance bridges (2 plates on each of 3 orthogonal coordinate axes). These three independent pairs of signals are used (in a control loop) to turn on (and off) three corresponding pairs of cold gas jets. Simply put: if the satellite approaches one side of the proof mass then the thrusters (on the opposite side) accelerate the satellite to restore the gap symmetry.

The thrust from a single jet is either on or off. Only the on-off modulation is changed by the nearness of the proof mass to the cavity wall. Among other advantages, this scheme minimizes the valve leakage and reliability problems.

It was intended that the satellite be placed in a near-circular orbit ($\varepsilon = 0.006$) at an average altitude of 874 km ($a = 1.1371$). Because of a malfunction of the launch vehicle guidance, the actual orbit has an average altitude of 788 km ($a = 1.1236$) and the correct eccentricity. This difference has had no significant effect on the DISCOS experiment.

A failure in the satellite telemetry system, two months after launch, has drastically reduced the aeronomy data of this particular experiment—but not before its promise had been shown. The DISCOS unit was on almost continuously from launch (Sept. 2, 1972) until mid-Sept. 1973 when it was deliberately turned off.

II. DISCOS Design

The design of the DISCOS was based on the performance specification of cancelling all nongravitational effects to a level of 10^{-11} g. The propulsion system was to operate on-off so a "deadband" was incorporated in the control signal. The proof mass was permitted to move ± 0.9 mm within this deadband; therefore, a consistent specification for the gradient in disturbing forces was established at 10^{-11} g/mm. Working from these specifications, the design requirement falls naturally into two categories: 1) to insure that the proof mass is not disturbed by any interaction with the satellite; and 2) to insure that the thrusters provide the necessary acceleration corrections.

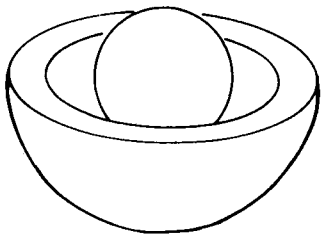

Fig. 3 Proof mass and cavity.

Functionally, the mechanization of the control system is shown in Fig. 4. An exploded view of the DISCOS as built is shown in Fig. 5. The configuration of the entire satellite was also influenced by the requirements that the proof mass perturbations be kept small.

Proof Mass Perturbations

Although the proof mass is shielded from the external surface forces which disturb the satellite, there are new disturbances introduced by the satellite itself. The principal one of these is the mass attraction of the satellite on the proof mass. All parts of the satellite which were not essential to the operation of the control system were located at the two extreme ends of the booms. It was necessary to divide the satellite into three bodies, rather than two, because the mass center of the satellite must be close to the proof mass, or there is unacceptable coupling between the attitude motions and the DISCOS translation control system. In the final configuration, the contribution to the mass-attraction uncertainty from the two end bodies was restricted to a few percent without requiring unusual fabrication tolerances or measurement accuracy in determining mass properties.

Not surprisingly, the parts closest to the proof mass were the most demanding. The proof mass pickoff housing had to be allotted a share of the error budget five times as large as any other single component. Initially, the pickoff housing represented 40% of the entire error budget from all sources. In spite of this, it was impossible to obtain the required density homogeneity in the beryllium oxide material (selected to insure acceptable performance electronically and thermally) to meet this mass attraction tolerance. As a consequence, the error budget had to be redistributed after the initial specifications had been written.

Mass attraction disturbances of major DISCOS components, e.g., the regulator, were calculated with great precision.[3] It was necessary to include the third moments of mass in an expansion around the regulator mass center. The parameters of the main term (mass) and the first correction term (involving the second moment of mass) can be experimentally verified by measuring the mass and the six elements of the moment of inertia. The third moment of mass had to be calculated from drawings of the component parts and weights that were determined during assembly. The location of the regulator involved an accumulation of tolerances from the pickoff housing through the upper support tube, the top lid, and the propulsion subsystem. These resulted in fabrication specifications as tight as 0.013 mm to

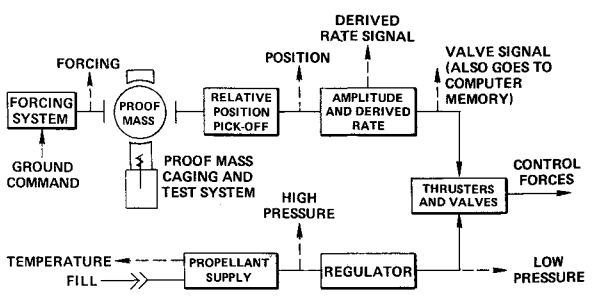

Fig. 4 Functional diagram of DISCOS control system.

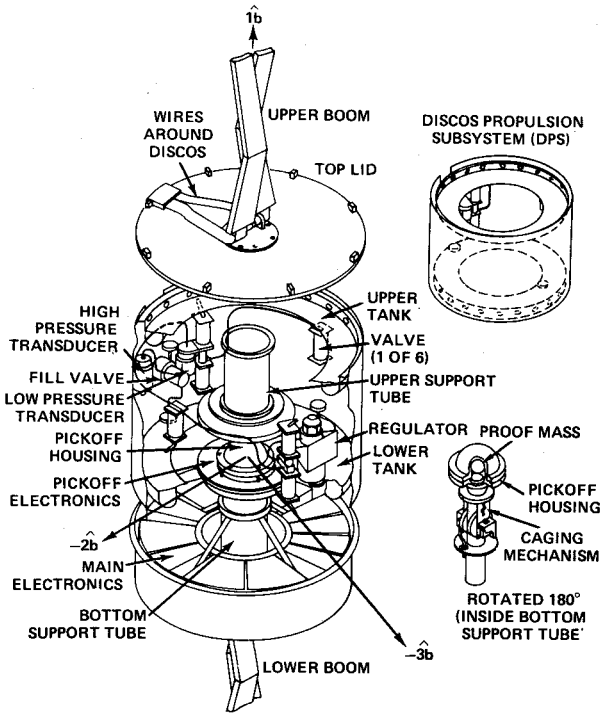

Fig. 5 Disturbance compensation system.

insure that the mass attraction was adequately modeled. Similarly, fabrication tolerances or measurements to 0.0025 mm were required in the fabrication of the pickoff housing and thickness measurement of the propellant tanks. The effect of the mass attraction of all parts of the satellite was calculated using measured values wherever possible.

Finally, a compensation mass was incorporated immediately above the pickoff housing. The residual mass attraction, before the compensation, was calculated as 83.6×10^{-11} g in the vertical direction but only 0.8×10^{-11} g in the more sensitive "along-track" (in the direction of the satellite velocity) direction. With the compensating mass, the maximum disturbance was calculated to be 2×10^{-11} g normal to the orbit plane but 0.7×10^{-11} g in the along-track direction. The compensated gradients were of the order of 2×10^{-11} g per mm.

Electric forces were kept to a much smaller value than the mass attraction forces. The excitation of the pickoff bridge was kept small enough that even with an unbalanced capacitive bridge, the expected forces would be (nearly) an order of magnitude smaller than the mass attraction forces. It is difficult to estimate the static charge that could accumulate on the proof mass in the space environment. We did not expect potentials that would be significant and our orbital performance to date verifies this assumption.

The magnetic gradient forces can be minimized by keeping magnetic fields small and by minimizing the magnetic susceptance of the proof mass. A contribution of no more than 10^{-13} g was insured by the choice of a material with a susceptance of 5×10^{-8} cgs units in the presence of a magnetic dipole of 100 pole cm at a distance of approximately 15 cm. The highly refined gold-platinum alloy exceeded these requirements.

Temperature gradients are important considerations in the design of the propellant tanks. The mass of a gaseous propellant is not distributed uniformly within the propellant tanks unless it is at a uniform temperature. To prevent the propellant migration from compromising the mass attraction specification, we maintained the temperature differences across the propellant tanks to less than 2°C.

The radiation pressure caused by the temperature differences in the pickoff housing was kept small by the selection of beryllium oxide as the pickoff housing insulator material. Beryllium oxide is unique among insulators in that it has excellent thermal conductivity.

Control System

Two pickoff techniques were evaluated in detail though many were considered. A capacitive bridge was chosen over optical techniques because of our previous laboratory experience with this type of sensor and because it presented an easier way of insuring acceptable mass attraction with minimal heat input. The bridges are excited by driving two pairs in common mode against the third pair. The third pair is driven at twice the potential of the other two so that the proof mass remains at ground potential. The excitation frequency was 1.031 MHz. To provide the necessary freedom of motion of the satellite with respect to the proof mass, a 9 mm gap was selected. This made the active capacity in the detector 0.3 pF; hence, the stability of shunt capacity to ground was extremely important. Pickoff null shifts were specified as 1 mm (or less) and no significant changes have been detected during flight.

The proof-mass position was measured and used as the command signal to a derived-rate[2] modulator. This type of control provides its own damping for transient settling and insures "good" limit cycle behavior when it is designed to have a nonlinear modulation factor. In the DISCOS, the equivalent linear gain-to-saturation is 25 times larger than the gain for small displacements past the deadband. The control stays full-on for any displacements larger than 6 mm.

The right-handed coordinate axes for the DISCOS control system were chosen as the along-track direction, and two directions perpendicular to that, 45° with respect to the vertical. This 45° rotation was necessary to provide thrust axes which do not interfere with the booms in the vertical direction. The capacitive plates (inside the pickoff housing) and the thrusters are located relative to this coordinate system so that each of the three axes is independent (in sensing *and* control) from the other two.

The propulsion subsystem is a conventional, cold gas propulsion system. The toroidal propellant tanks, however, were necessary to satisfy the satellite mass-attraction requirements. As the propellant mass decreases with time, *changes* in its mass center, changes in its center of attraction, and gradient in its mass attraction (at the proof mass) must remain zero at all times. A gaseous propellant which distributes itself uniformly through the tanks does not require special propellant containment. At least two tanks are needed to provide a mass center at the proof mass and also keep the gradient sufficiently small. (The gradient within a uniform, hollow, spherical, mass shell is zero.) The two toroids provide an approximation to the uniform shell and for the configuration used in DISCOS satisfied the requirements for zero attraction and near-zero gradient of mass attraction from the propellant at all times.

The pressure regulator is a two-stage one which insures that any two-phase flow in the freon gas passing through its initial pressure drop, is properly regulated in the second stage. No difficulties were experienced in ground tests (or in flight) with the freon gas. The 1.4 kg of gas provided a (nominal) total impulse of 600 Nsec.

The control acceleration needed to combat external disturbances is (on the order of) 10^{-8} g for this satellite. Initial transient settling requires an order-of-magnitude larger thrust to be at all practical. Existing regulators were not available to provide regulated pressure below one atmosphere; moreover, thruster throat diameters become overly sensitive to contamination (and difficult to fabricate) if made much smaller than 0.25 mm in diameter. Because of these practical constraints, we were forced to accept a larger thrust than was necessary. As a result, the thrust duty cycle is approximately 0.1%. The maximum control acceleration is approximately 10^{-5} g and varies as much as 20% with each of the thrusters according to the actual diameter of its nozzle.

The entire DISCOS including its electronics, some telemetry and common electronics, also housed in the DISCOS package,

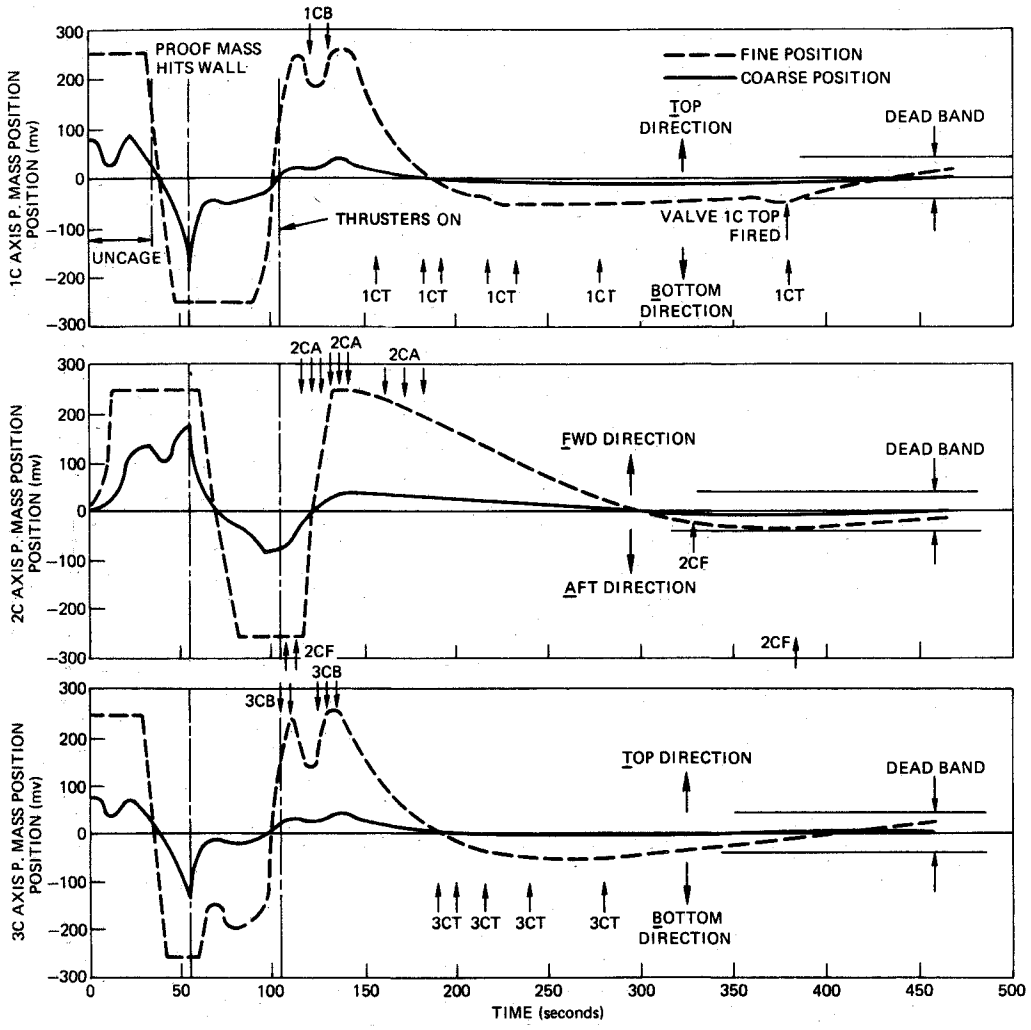

Fig. 6 DISCOS proof mass uncaging.

weighs 10.6 kg and consumes less than 3 w. It was expected to operate for more than a year before the propellant was depleted. This expectation was realized.

Forcing System

To cancel bias which might be observed and to provide for orbit adjustments, a proof-mass forcing system was included. Electrostatic forces can be applied to the proof mass by placing a d.c. bias potential on the fore or aft plates of the along-track sensing bridge. The maximum design acceleration is approximately 10^{-8} g and the smallest is approximately 10^{-12} g. There are 255 equal steps in $\pm$ voltage which gives a nonlinear range of values of forcing with greater resolution at the smaller accelerations.

III In-Orbit Performance

In attempting to answer the question: "How well did we meet our design goals?" we used both the telemetry data and Doppler tracking data.[4-7] The former enabled us to confirm that the control loop was stable and that the ball was in free flight in the cavity.

This stability was established immediately after the satellite was placed in orbit and the ball "uncaged." The ball-capture sequence is shown in Fig. 6. All three components of the ball position are shown as functions of time. As is clear from the figure, the capture-sequence transient has disappeared after 240 sec.

A sample of the vector ball position data is shown in Fig. 7. By fitting second-order polynomials to the data, the acceleration of the ball relative to the satellite can be determined. In the absence of ball interaction with the satellite, this acceleration is entirely due to the surface forces acting on the satellite. This is a source of high-precision aeronomy data, particularly when the satellite is in the dark.[8]

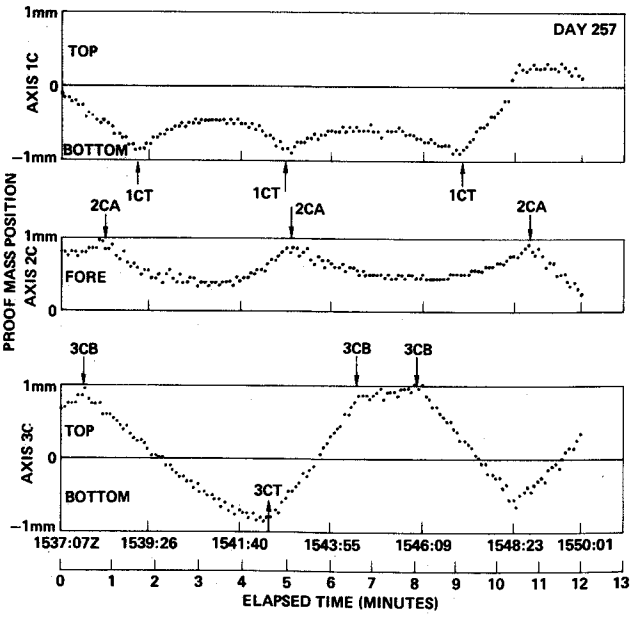

Fig. 7 DISCOS proof mass position.

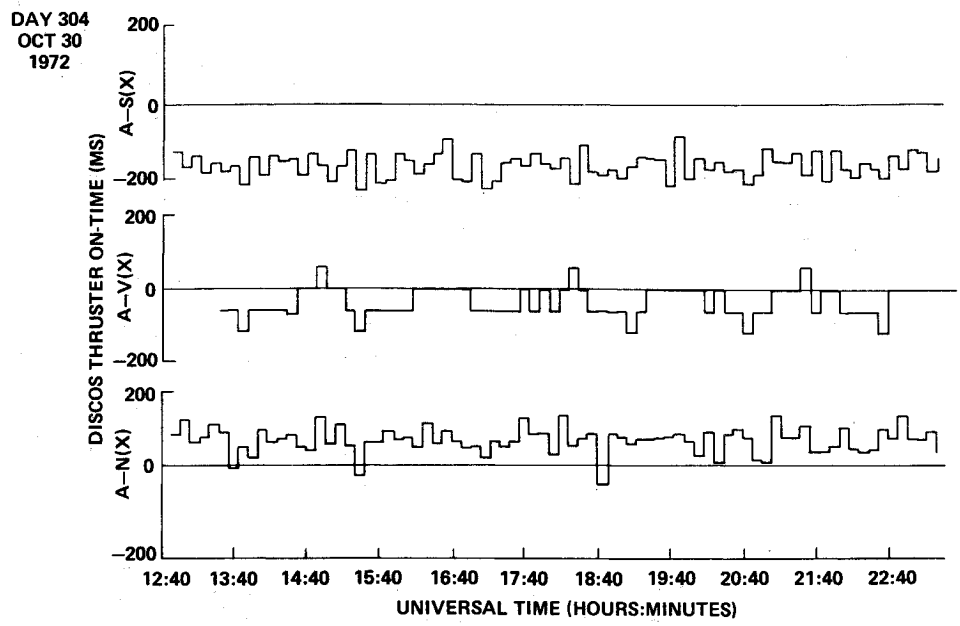

Fig. 8 Smoothed thruster data from day 304 72.

The discontinuities in the parabolas correspond to thruster firings. From the associated velocity discontinuities, an in-orbit calibration of the thrusters can be obtained. In the failure of the TM system, however, we lost a large body of valuable aeronomy data. We have concentrated our efforts on the tracking data (described in Sec. IV) and the thruster "on-time data."

The telemetered DISCOS data includes, for each of the 6 thrusters, the accumulated, commanded, on-time in every four-minute interval.* It was fortunate that the data contained a day when the sun was nearly normal (81°) to the orbit plane. For this particular date, the radiation pressure and drag forces were nearly orthogonal. The cross product of these two vectors is nearly in the direction of the satellite position vector. A resolution of the thruster on-time data in these three directions is shown in Fig. 8. The top curve is the component along the satellite-sun line. The center curve is the component along the satellite velocity vector and the bottom curve is the component along the satellite position vector. The top curve shows radiation pressure, the center curve shows drag.

The extreme values on the ordinate (200 msec) correspond to a total impulse of 170 dyne-sec. There are several things apparent from the data. 1) The drag force is, on the average, only $\frac{1}{5}$ as large as is the radiation pressure. 2) The drag force has (consistent with the Jacchia model[6,10] and the polar orbit) a strong orbital frequency component. 3) Surprisingly, there is a rather large radial bias force.

This last observation triggered an intensive search for the source of the bias. The most likely cause is the center of mass of the entire satellite does not lie at the center of the proof-mass cavity. As a result, the proof mass and the satellite are in different orbits. To follow the proof mass, a thrust component along the vertical is required due to the gradient in the Earth's field. The most probable origin of this bias is a 1 cm maladjustment in one of the boom lengths. (The boom lengths were to

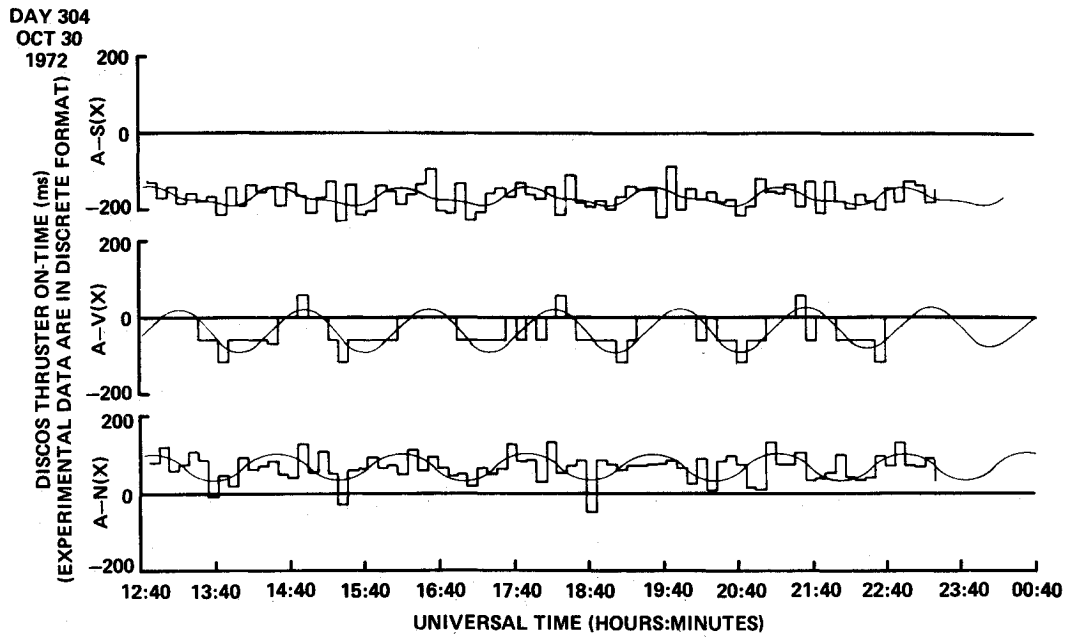

Fig. 9 Experimental data vs simulated data, day 304.

* The actual thruster on-time is proportional to the total impulse.

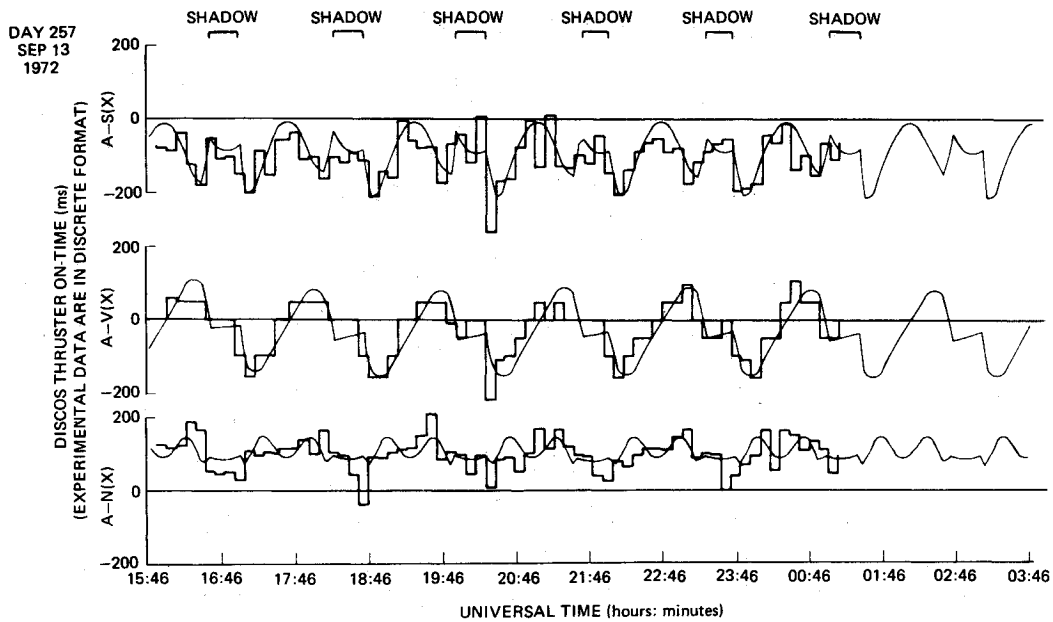

Fig. 10 Experimental data vs simulated data, day 257.

have been adjusted in orbit and, had the telemetry system not failed, this bias would have been removed.)

We used a computation of the radiation pressure to derive the relationship between "calibrated" thrust and in-orbit thrust. From this thrust, the radial acceleration bias is $3–5 \times 10^{-9}$ g.

Finally, we used models of the drag force, radiation pressure (and bias) and computed the three acceleration components and compared them with the data. The results of the comparison are shown in Fig. 9 for the day 304 data and in Fig. 10 for the day 257 data. In the day 257 data, the satellite-sun relative geometry has appreciably changed and moreover, our three coordinate components are no longer near orthogonal. Even so, the calibration achieved on day 304 remains valid.†

IV. TRIAD Tracking Experiments

The objectives of the TRIAD tracking experiments were to test the satellite ephemeris predictability, and to determine the level of the self-bias force present in the DISCOS unit. The experiments have two phases: short-arc predictions with maximum time spans of 2 to 3 weeks, and long-arc predictions with time spans of several months. The long-arc experiments have not been completed and will not be reported on here.

To perform the experiments and also to provide a continuous span of tracking data over one complete revolution of perigee for future geodesy purposes, the DISCOS system was kept in the active state without interruption for 5 months. This period began on Oct. 18, 1972 and ended on March 13, 1973. During that time the proof mass did not touch the cavity wall, so the effects of drag and radiation pressure were completely eliminated. The satellite Doppler data were continuously recorded by the TRANET system of 13 world-wide stations. They averaged about 35 usable Doppler passes per day during the 5-month span.

The ephemeris accuracy was measured by station navigation using a predicted ephemeris. The navigation process partitions the ephemeris errors for each Doppler pass by simultaneously fitting a station position and a mean satellite frequency "offset" to the Doppler residuals. The Doppler data residuals are obtained by computing the theoretical Doppler shift using the predicted ephemeris. The movement of the station location in this fit resolves the ephemeris errors into the "along-track" and the "slant-range" directions. (The slant-range direction is determined by the vector from station to satellite at time-of-closest approach. The along-track direction is normal to the slant-range in the direction of satellite motion.)

Unmodeled or incorrectly modeled forces can be related to the along-track and slant-range ephemeris errors by appropriate orbit perturbation techniques. The algebra is fairly complicated, so only the important qualitative behavior will be mentioned here. In particular, the main effect of an unmodeled along-track force bias is a *quadratic* growth of the along-track navigation error. For a self-bias force of 10^{-11} g, the growth would be about 110 m in 10 days. In 30 days the error would grow to about 1 km.

The results for one of the early 2 week prediction spans is shown in Fig. 11. Each point in the figure represents a single 15 min Doppler pass for a TRANET site. The predicted ephemeris was based on a 2-day data span for days 312–313, 1972.

To improve these results and to obtain a reliable estimate of the DISCOS self-bias force, we had to solve four different problems. 1) Correct errors in the Earth-gravity zonal harmonics. 2) Correct certain resonance, nonzonal harmonics. 3) Correct for the difference in rates of UT1 and UTC. 4) Correct errors in the numerical integration process used to generate the ephemeris.

1) Zonal Harmonic Effects

In along track and slant range, the effect of an error in a zonal harmonic causes (mainly) orbital frequency error having a secular and long period envelope. There is also a contribution to the along-track error, due to the odd degree zonals, which resembles a long period (120-day) cosine curve. Over a short arc, this can easily be confused with the quadratic error growth expected from a self-bias force. The APL 5.0-1967 gravity model[5] contains zonal harmonics up to degree 12. Using the data span in Fig. 11, one additional even (and odd) degree zonal harmonic were determined from the navigation data and their effects subsequently removed.

2) Nonzonal Resonance Terms

The main importance of correcting for the errors in the resonance terms is that they can cause the satellite period to be poorly determined in a short-arc track. The principal, nonzonal resonance term for TRIAD is of 14th order, with a characteristic period of 3.82 days; a weaker resonance with the 15th order harmonics has a period of 1.35 days. An along-track, 3.82 day resonance error (20-m amplitude) was corrected with an odd degree-14th order nonzonal. The smaller, 10-m amplitude term was corrected with an odd degree-15th order nonzonal. At the

† It has been suggested that the infra-red radiation from the Earth is responsible for part of the radial bias. Computation shows that this effect is a factor of 10 too small to account for what we measure.

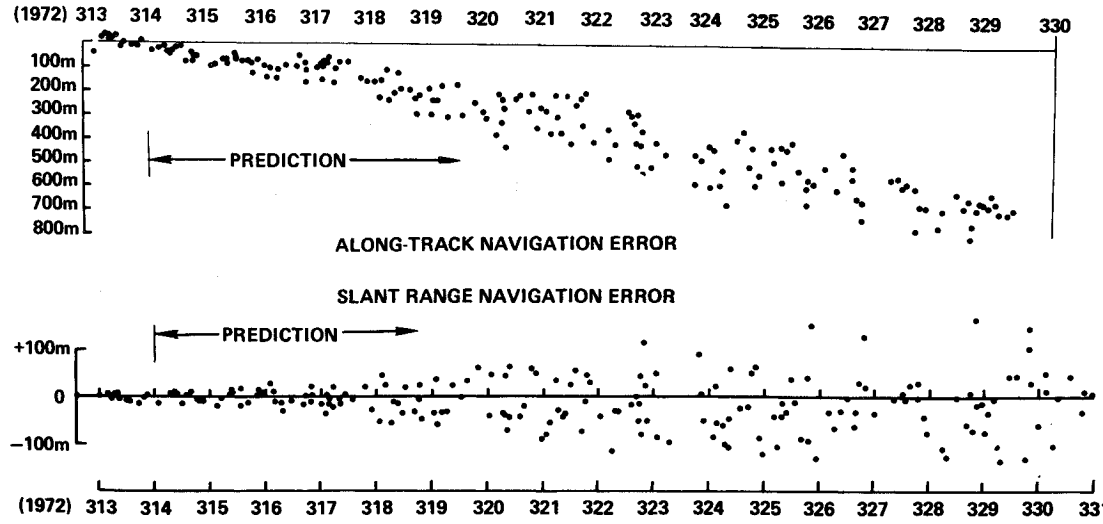

Fig. 11 Navigation errors with predicted ephemeris.

present time, with the other errors removed, there appears to be a relatively small, 2.5-day resonance effect coming from the 28th order harmonics; although we have not yet tried to determine it.

3) Correction for UT1 Rate

The time base for the data collection and the orbit integration is UTC, which now has the uniform rate of A.1 atomic time. The UT1 time is required to determine the correct station position in inertial space at the time of a pass. That is, it is not sufficient to predict the satellite orbit in inertial space, but to evaluate the errors, we must also predict the orientation of the earth under the orbit. Over a short arc (several days), the difference between UT1 and UTC is nearly constant and can be ignored, the net effect being the generation of a bias in the longitude of the node. Over long arcs, the drift in the differences, UT1-UTC, causes an apparent shift in the node which cannot be superficially removed. During the time span in Fig. 9, the difference UT1-UTC changed about 70 msec causing an apparent shift in the node of about 5×10^{-6} rad. The effect becomes more important the longer the span, but the BIH-extrapolated rates are good enough to reduce the error to a few meters for predictions as long as six months.[9]

4) Numerical Integration Errors

The results shown in Fig. 11 are based on a satellite ephemeris generated by numerical integration in Cartesian space. The method used is an 8th-order Cowell integration using the Adams-Moulton multistep predictor-corrector technique and a Runge-Kutta start up. For computational efficiency, we have also developed an analytic, seminumerical ephemeris generator for use in long-arc predictions and data analysis. This method computes the short period perturbations (those depending on the phase of the satellite in orbit) by the standard second-order analytic technique, and numerically integrates the long period (and secular) effects with a time step of one satellite revolution. Although we had considerably more confidence in the precision of the numerical integrator for short arcs, we were surprised to find that the analytic method did considerably better over the 17-day arc in Fig. 11. (The differences in the peak errors were nearly 50 m.) By all measures we have made,‡ the numerical

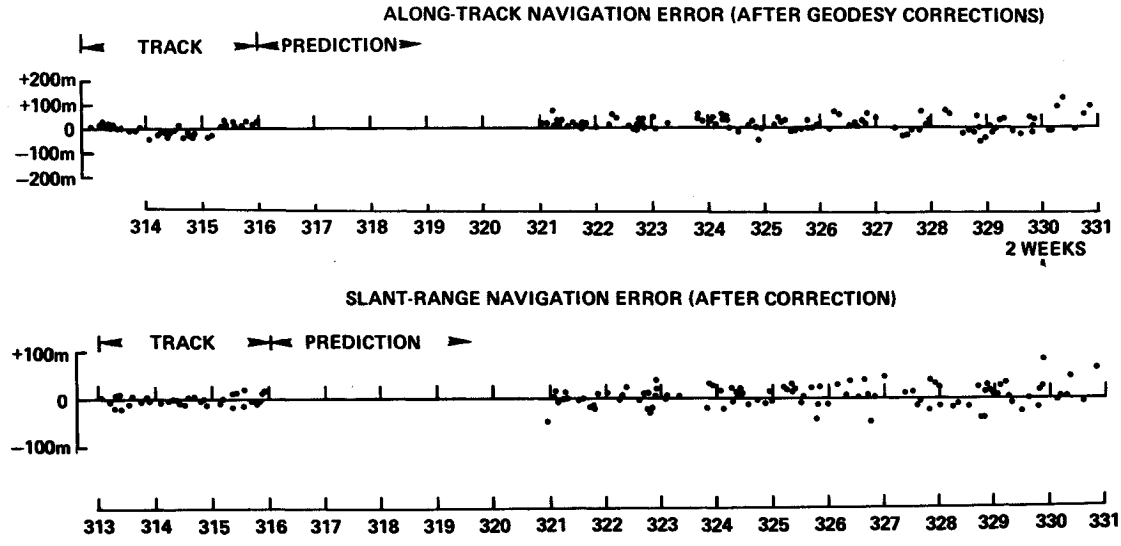

Fig. 12 Navigation errors with predicted ephemeris (after corrections).

‡ Tests include: integrating a pure Kepler orbit, testing the Jacobi Energy Integral with the full gravity field, closure, and self-consistency with different time steps.

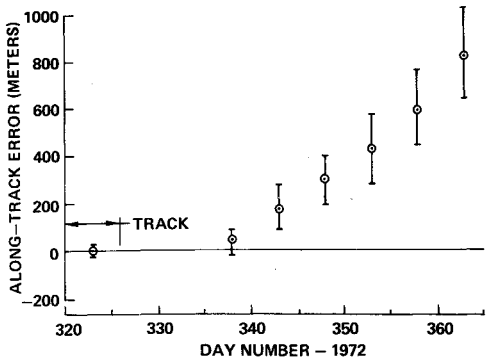

Fig. 13 Along-track orbit errors.

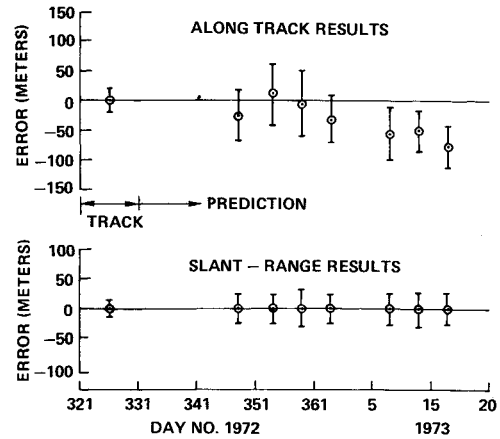

Fig. 14 Orbit errors for 60-day prediction with modeled bias force of 5.5×10^{-12} g.

errors with an integration step of 60 sec should be no more than a few meters in 17 days. We have concluded that there is an error in computing one of the small forces in the numerical integrator which we have not yet uncovered.

In determining the above corrections for the zonal harmonics and the resonance terms, the value of TRIAD for geodetic purposes became apparent. The low (788 km) altitude of the satellite, together with the removal of surface force effects, resulted in valuable geodesy data. The lower altitude serves to amplify the higher-degree gravity perturbations, and it also provides (even though it is a polar orbit) a new linearly independent equation for a geodesy solution. This was emphasized by the fact that our gravity set (APL 5.0-1967,[5]) which works well for polar satellites at 1100 km altitude was not well matched to the TRIAD orbit. TRIAD showed a 50% degradation in the short-arc tracking precision when compared with polar satellites at 1100 km!

Figure 12 shows the prediction errors over the same span as Fig. 11 *after* the above corrections were applied. The ephemeris used in Fig. 12 was generated by the analytic technique rather than numerical integration. Also, the tracking span to start the prediction was increased to three days (313–316) to improve the period determination.

The results are much improved. The errors after a two week prediction are still on the order of 100 m, and there is no evidence of an along-track self-bias force as large as 10^{-11} g. However, there are still "growing" type errors which we have not completely eliminated.

The geodesy corrections applied to obtain Fig. 12 were not accomplished in a way to fundamentally improve our gravity model, but rather, were simply ad hoc alterations to improve the TRIAD orbit precision. That is, all of the different degree harmonics for a given order were not adjusted to reflect the TRIAD data, so that the added coefficients apply only to the TRIAD orbit. By reconstructing the equations of condition for the APL 5.0-1967 geodesy set, and adding the TRIAD corrections in the form of additional equations, it is possible, by resolving the set of normal equations, to obtain an over-all improvement in the actual geopotential model.

The next step was to increase the prediction span to 40 days (and 40 nights). With this length span, it is more convenient to test the predicted ephemeris at intervals, rather than continuously, along the span. Accordingly, the navigation tests were made with a day's worth of passes (about twenty) every fifth day. Figure 13 shows the resulting along-track error. The ephemeris was predicted from a 10-day track (days 321–331). The plotted points are the average along-track errors for the passes navigated over that day. The bars show the limits on the rms "scatter" for the passes that day. The slant-range results are not plotted, but they had about the same magnitude scatter.

There is clearly a quadriatic along-track error growth in Fig. 13. This growth is consistent with a constant along-track self-bias force of about 5×10^{-12} g. To test this, a constant along-track force of this magnitude was modeled in the orbit integration program, and the test was repeated with a still longer prediction span. These results are shown in Fig. 14. Again, each point plotted is based on the average navigation results of about 20 passes.

Although the quadriatic effect has been removed, there are still structured, secular errors in the predicted orbit. The origin of at least a portion of this secular error is understood. Some error is due to an orbit period error, and some is due to residual errors in the zonal harmonics.

References

[1] Lange, B., "The Drag-Free Satellite," *AIAA Journal*, Vol. 2, No. 9, Sept. 1964, pp. 1590–1606.

[2] Nicklas, J. C. and Vivian, H. C., "Derived Rate Increment Stabilization: Its Application to the Attitude Control Problem," *Transactions of the ASME; Journal of Basic Engineering*, Sec. D, Vol. 84, March 1962, pp. 54–60.

[3] Fleming, A. W. and Tashker, M., "Mass Attraction of TRIAD I/DISCOS," Rept SUDAAR 445, Sept. 1972, Stanford Univ., Stanford, Calif.

[4] Eisner, A. and Yuhasz, R., "A Flight Evaluation of the DISCOS System on the TRIAD Satellite," JHU/APL TG-1216, April 1973, The Johns Hopkins Univ., Applied Physics Lab., Silver Spring, Md.

[5] Yionoulis, S., Heuring, F. T., and Guier, W., "A Geopotential Model (APL 5.0-1967) Determined from Satellite Doppler Data at Seven Inclinations," *Journal of Geophysical Research*, Vol. 77, No. 20, July 10, 1972, pp. 3671–3677.

[6] Jacchia, L. G., "Static Diffusion Models of the Upper Atmosphere with Empirical Temperature Profiles," *Smithsonian Contributions to Astrophysics*, Vol. 8, No. 9, 1965, pp. 215–257; see also Ref. 10.

[7] *APL Technical Digest*, Vol. 12, Nos. 2 and 3, 1973. (The entire issues are devoted to the TRIAD satellite results.)

[8] Moe, O. K., "Deduction of Atmospheric Densities from the DISCOS Data Collected by the TRIAD Satellite," McDonnell Douglas Final Rept. under letter agreement PR 1637 under APL/JHU 271881, Aug. 1973, Applied Physics Lab., Silver Spring, Md.

[9] Muller, I. I., *Spherical and Practical Astronomy as Applied to Geodesy*, Ungar, New York, 1969, (see esp. Chap. 5); see also Circular D of the Bureau International deL'Heure (B.I.H.), Paris, France.

[10] Jacchia, L. G., "Revised Static Models of the Thermosphere and Exosphere with Empirical Temperature Profiles," Special Rept. 332, May 5, 1971, Smithsonian Astrophysical Observatory, Cambridge, Mass.; (see also *COSPAR International Reference Atmosphere Akademie*, Verlag, Berlin, 1972.)